THE ASTROPHYSICAL JOURNAL, 463:310–319, 1996 May 20

SOURCES OF THE 13 MICRON FEATURE ASSOCIATED WITH OXYGEN-RICH CIRCUMSTELLAR DUST

G. C. SLOAN
NASA Ames Research Center, MS 245-6, Moffett Field, CA 94035-1000; sloan@ssa1.arc.nasa.gov
P. D. LEVAN
Phillips Laboratory/VTRP, 3550 Aberdeen SE, Albuquerque, NM 87117-5776; levan@smtpgw1.plk.af.mil
AND
I. R. LITTLE-MARENIN
Whitin Observatory, Wellesley College, Wellesley, MA 02181; ilittle@casa.colorado.edu
Received 1995 October 27; accepted 1995 December 15

ABSTRACT

A search of the database of spectra from the *IRAS* Low-Resolution Spectrometer has revealed 13 μm emission features in 187 sources, most of which are associated with stars embedded within oxygen-rich circumstellar dust shells. Our sample is very incomplete, but we estimate that 40%–50% of all sources with oxygen-rich dust on the asymptotic giant branch (AGB) exhibit emission features at 13 μm. The similarities of the Galactic distribution, mean radial velocities, infrared colors, and other properties of the sample of 13 μm sources compared to the parent population of variables on the AGB suggest that the carrier of the 13 μm feature is commonly produced in oxygen-rich dust environments. A strikingly large fraction of SRb variables show 13 μm features, approximately 75%–90%, which suggests that the formation and/or survival of the carrier of the 13 μm feature may be enhanced by the unusual pulsational properties of these variables.

Subject headings: circumstellar matter — infrared: stars — stars: AGB and post-AGB

1. INTRODUCTION

Following the initial discovery and identification of silicate emission from circumstellar dust shells at 10 μm (Gillett, Low, & Stein 1968; Woolf & Ney 1969; Gilman 1969), some infrared spectroscopists hinted that other types of oxygen-rich dust might modify the shape of the classic silicate emission feature (Hackwell 1972; Treffers & Cohen 1974; Forrest, Gillett, & Stein 1975). But the extensive program of infrared spectroscopy by Merrill & Stein (1976a, b, c) indicated that most, if not all, of the differences seen in silicate spectra could be attributed to differences in the optical depth of the dust. In this picture, as the optical depth of the shell increases, the classic emission feature would flatten, self-absorb, and finally become the strong absorption feature seen in heavily obscured infrared sources and H II regions such as the Trapezium region in the Orion Nebula (Gillett et al. 1975).

The tremendous number of infrared spectra obtained by the Low Resolution Spectrometer (LRS) aboard *IRAS* changed this picture. Ossenkopf, Henning, & Mathis (1992) derived optical constants for classic circumstellar silicate emission from the LRS data and demonstrated that the spectral emission from circumstellar and interstellar silicates showed significant differences. Their constants are much more appropriate for circumstellar silicates than constants derived from dust emission in the Trapezium region of Orion (Draine & Lee 1984; Draine 1985). Careful analyses of LRS measurements have also revealed many spectra from oxygen-rich circumstellar dust that diverge significantly from the classical circumstellar silicate profile (Little-Marenin & Price 1986; Vardya, de Jong, & Willems 1986; Onaka, de Jong, & Willems 1989; Little-Marenin & Little 1988, 1990; Simpson 1991).

Vardya et al. (1986) and Onaka et al. (1989) argued that differences in the dust composition of circumstellar shells must account for at least some of the variations observed. Onaka et al. (1989) suggested that the low-contrast, broad emission feature that peaks at wavelengths of 11–12 μm arises not from silicates, but from alumina material (Al_2O_3). Little-Marenin & Little (1988, 1990, hereafter LML) developed a classification system for the various types of spectra observed, which recognized six distinct classes of circumstellar dust emission. Their Silicate+ and Silicate++ classes include those sources in which the silicate emission feature at 10 μm is accompanied by an additional emission peak at 11 μm. This emission, sometimes described as structured silicate emission, has been attributed to crystalline forms of silicate grains (Tielens 1989; Little-Marenin & Little 1990; Nuth & Hecht 1990) because of the similarity with spectra from crystalline silicates in interplanetary dust particles (Sandford & Walker 1985) and in comets (e.g., P/Halley; Bregman et al. 1987).

Sloan & Price (1995, hereafter Paper I) examined the shape of dust emission using ratios of the dust emission at 10, 11, and 12 μm and found that the sequence from broad to classic emission represented a very smooth progression of spectral shape. They used this silicate dust sequence, as they called it, to define a Silicate Emission (SE) index, an alternative to the LML classification. The silicate dust sequence is divided into eight segments indexed 1–8, with broad emission corresponding to SE1–2 and narrow emission corresponding to SE7–8. Intermediate SE indices represent intermediate emission types described by LML as Silicate+ and Silicate++.

According to Stencel et al. (1990), the different spectra from oxygen-rich dust may represent stages in the compositional evolution of dust grains as shells form and grow. They suggested that dust evolved from alumina to silicate, or from broad emission to structured and then to classic

silicate emission. Alternatively, the variations in grain composition may result from different physical conditions in the dust formation region (e.g., Tielens 1989). Thus, the shape of the infrared spectrum from the dust may depend on the evolutionary state of the dust shell or on physical properties of the central star (e.g., mass, composition, and pulsation mode).

The LRS measurements have also resulted in the discovery of an additional emission feature at 13 μm. Little-Marenin & Price (1986) first discussed this feature, although it had appeared without comment in previously published spectra (e.g., T Cas as observed by Forrest et al. 1975). This feature probably escaped previous recognition in ground-based spectra because it occurs at the edge of the N-band window, where poor atmospheric transmission makes it difficult to obtain good data from the ground. In their study of LRS data, Little-Marenin & Little (1988) noticed that the 13 μm feature usually appeared in conjunction with emission peaks at 10 and 11 μm and used this feature as a criterion of what they called the three-component class of oxygen-rich dust emission. Paper I, however, found that the 13 μm emission can be associated with almost any type of oxygen-rich circumstellar dust; it can be seen in spectra from anywhere on the silicate dust sequence.

We have chosen to investigate the 13 μm emission feature in the hope that it may help address some of the continuing uncertainties about the formation and composition of circumstellar dust shells in general. We also hope to provide clues that may lead to a firm identification of this enigmatic feature. Our immediate goal is to constrain the carrier of the 13 μm emission feature by determining what type of source produces it. In § 2, we define the sample of sources that exhibit this feature, and in § 3 we confirm its existence in ground-based spectra. The limits to our sample are discussed in § 4, while § 5 is devoted to investigating how our sample of 13 μm sources differs from the larger population of evolved stars associated with oxygen-rich dust.

2. THE SAMPLE

Paper I defined a sample of variables associated with the asymptotic giant branch (AGB), by cross-referencing the General Catalogue of Variable Stars (Kholopov et al. 1985–1988, hereafter GCVS) and the *IRAS* Point Source Catalog (1988, hereafter PSC). These variables include Miras, semiregulars (types SRa and SRb), and irregulars of type Lb, all associated with the AGB (Hoffmeister, Richter, & Wenzel 1984). The spectrum of each source was obtained from the LRS database and analyzed. Paper I provides additional details on recalibration and analysis, but we should repeat the description of the search for the 13 μm emission feature. We fitted a polynomial to each spectrum over the wavelength ranges 10.66–12.59 μm and 13.72–15.18 μm and measured the excess emission in between (12.70–13.41 μm). We found that a high-order polynomial was necessary to fit the complicated dust spectrum; we used both five and six degree polynomials. To obtain a rough estimate of the noise in the spectrum, we calculated the rms deviations from the polynomial in the wavelength range 10.66–12.59 μm. Figure 1 illustrates this method for some representative spectra.

We detected a 13 μm feature if and only if (1) both polynomials produced a 4 σ detection and (2) one of the polynomials resulted in a feature with a strength of 5% of the background spectrum or more. To these two constraints used in Paper I, we add a third: the uncertainty in the strength of the 13 μm feature must be less than 5% of the integrated continuum flux. This constraint removes a few extremely noisy or spiky 13 μm features from our sample; we doubt that any of them are real. In particular, it slightly modifies the results quoted in Paper I by eliminating one SRb variable as a 13 μm source. Of the sample of 546 oxygen-rich AGB sources, 128 are found to contain 13 μm emission features. All but three are among the 453 AGB sources associated with emission from oxygen-rich dust; these three were classified as naked in Paper I, but they probably contain excess emission with very low contrast (i.e., $<4\%$).

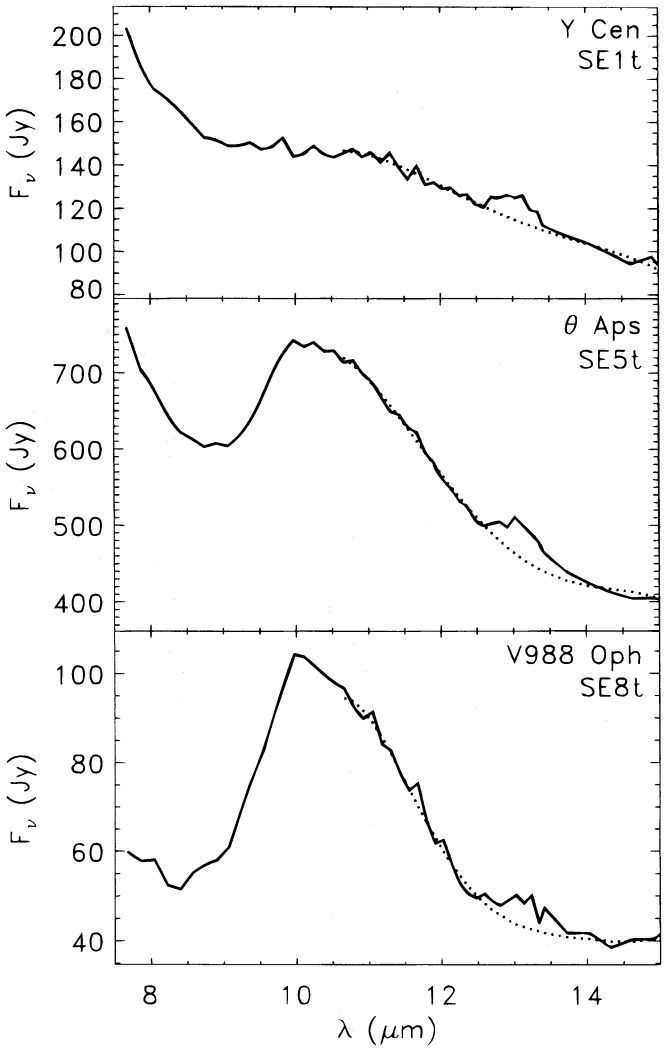

FIG. 1.—Examples of extractions of the 13 μm emission from three spectra. The dotted lines represent the polynomials fitted to the spectrum to isolate the feature, which is summed from 12.70 to 13.41 μm. We designate 13 μm sources by adding a "t" after the SE index.

Additional sources in the LRS database also show 13 μm features. By cross-referencing the GCVS and PSC for bright supergiant variables ([12] < 0.0; $F_{12} > 28$ Jy), we find 27 Lc and 37 SRc variables. We analyzed these as described above, finding 13 additional 13 μm sources. To search for further candidates, we examined the LRS Atlas (*IRAS* Science Team 1986) by hand. For each of the suspects, we analyzed the spectrum from the LRS, finding 46 additional 13 μm sources and raising our total count to 187 known sources with 13 μm features. These sources are listed in

TABLE 1

IDENTIFIED 13 MICRON SOURCES

IRAS PSC	Name	Type of Variable	Spectral Type	[12]	[12] − [25]	F_{11}/F_{12}	F_{13}/F_c	Dust Type
00192−2020.....	T Cet	SRc	M5–6S IIe	−2.11	0.19	0.76 ± 0.13	5.4 ± 0.7	SE1t
00245−0652.....	UY Cet	SRb	M7	−1.53	0.83	1.10 ± 0.05	9.0 ± 1.2	SE3t
00541+4825.....	KS Cas	SRa	M5	−0.08	0.66	1.14 ± 0.25	15.3 ± 2.9	SE3t
01438+1850.....	SV Psc	SRb	M5	−1.08	0.85	1.29 ± 0.08	10.0 ± 1.5	SE5t
01556+4511.....	HD 11979	...	M7 III	−3.12	0.98	1.18 ± 0.02	9.1 ± 1.1	SE4t
02000+0726.....	BD +06 319	...	M8	−1.35	0.71	1.15 ± 0.11	9.1 ± 1.9	SE4t
02188+5652.....	RS Per	SRc	M4 Iab	−1.05	1.08	1.33 ± 0.04	9.0 ± 1.5	SE5t
02192+5821.....	S Per	SRc	M3–7 Iae	−2.70	1.15	1.20 ± 0.03	8.1 ± 1.0	SE4t
02427−5430.....	W Hor	SRb	Mc	−2.01	0.91	1.10 ± 0.02	8.0 ± 1.6	SE3t
02464−5915.....	X Hor	SRa	M6–8e	−0.79	0.55	0.80 ± 0.13	6.1 ± 1.1	SE1t
02469+5646.....	W Per	SRc	M3–7 Ia–Iab	−1.26	1.41	1.30 ± 0.03	9.2 ± 1.1	SE5t
02522−5005.....	R Hor	M	M5–8 II–IIIe	−3.53	0.64	1.33 ± 0.03	4.8 ± 1.0	SE5t
02532+5426.....	ER Per	SRb	M6.5	−0.96	0.72	1.34 ± 0.29	15.2 ± 2.7	SE5t
02587+2136.....	UZ Ari	Lb:	M8	−0.17	0.69	0.83 ± 0.13	18.0 ± 2.2	SE1t
03030+5532.....	IO Per	Lc	M3 Iab	−2.32	1.28	1.32 ± 0.02	7.4 ± 0.9	SE5t
03040−8013.....	NSV 01045	NSV	...	0.09	0.63	0.84 ± 0.16	10.8 ± 1.8	SE1t
03172−2156.....	τ Eri	Lb	M3 III	−1.90	−0.02	0.58 ± 1.15	6.2 ± 0.9	Nt
03490+4455.....	BD +44 806	...	M7	−0.43	0.95	1.17 ± 0.10	17.5 ± 2.2	SE4t
03505−0919.....	SW Eri	M	M9	−0.39	0.63	1.45 ± 0.08	14.4 ± 2.2	SE6t
03507+3623.....	IRC +40072	var	M8	0.16	0.94	1.22 ± 0.12	15.3 ± 3.6	SE4t
04020−1551.....	V Eri	SRc	M6 II	−2.65	0.94	1.08 ± 0.03	8.1 ± 1.5	SE3t
04166+4056.....	IR Per	SRa	M6.5–9	−2.10	0.96	1.22 ± 0.01	9.1 ± 1.2	SE4t
04265+5718.....	RV Cam	SRb	M4–6 II–III	−0.79	0.99	1.40 ± 0.08	8.2 ± 1.3	SE6t
04280+2722.....	V729 Tau	SRb	M6	−0.43	0.87	0.90 ± 0.12	10.4 ± 2.0	SE1t
04328+2824.....	IU Tau	SRa	M7	−0.71	0.59	0.95 ± 0.10	7.8 ± 1.6	SE1t
04330−6307.....	R Ret	M	M4–7.5e	−0.20	0.45	1.03 ± 0.28	17.2 ± 2.8	SE2t
04355+0814.....	RX Tau	M	M6–7e	−1.00	0.63	0.92 ± 0.06	4.6 ± 0.9	SE1t
04361−6210.....	R Dor	SRb	M8 IIIe	−5.65	0.29	1.47 ± 0.07	8.6 ± 0.9	SE7t
04382−1417.....	BX Eri	SR	M2–7	−1.42	0.83	1.04 ± 0.04	10.6 ± 1.1	SE2t
05176−1755.....	BD −18 1061	...	M7	−0.29	0.95	1.19 ± 0.07	12.7 ± 1.7	SE4t
05220−0611.....	EX Ori	Lb	M7 IIIe	−0.51	0.85	0.98 ± 0.09	12.2 ± 2.1	SE2t
05365−1404.....	RW Lep	SRa	M8	−0.98	0.68	0.82 ± 0.14	10.8 ± 1.7	SE1t
05384+3854.....	SZ Aur	M	M8e	−0.84	0.57	1.04 ± 0.08	10.1 ± 1.7	SE2t
05390+1448.....	FX Ori	SRb	M3	−0.22	0.91	1.57 ± 0.11	23.6 ± 3.6	SE8t
05528+2010.....	U Ori	M	M6–9.5e	−3.46	0.51	1.37 ± 0.03	5.6 ± 1.7	SE6t
05534+4530.....	TW Aur	SRb	M5 III	−1.67	0.75	1.36 ± 0.05	7.0 ± 1.2	SE6t
05588+1054.....	DP Ori	SRb	M6.5	−0.38	0.67	1.11 ± 0.11	12.0 ± 1.4	SE3t
06036−2411.....	S Lep	SRb	M5–6 III	−2.40	0.90	1.42 ± 0.02	8.8 ± 0.8	SE6t
06092+2255.....	BU Gem	Lc	M1–2 Ia–Iab	−1.10	1.02	1.23 ± 0.04	4.9 ± 1.0	SE4t
06139+3313.....	VW Aur	SRb	M6	−1.44	0.81	1.20 ± 0.04	9.0 ± 1.3	SE4t
06140−2729.....	IRC −30005	...	M7 III	−0.93	0.72	1.21 ± 0.05	12.9 ± 1.2	SE4t
06250+6134.....	V Lyn	SRb	M5 III–IV(S:)	−0.34	1.20	1.32 ± 0.11	11.7 ± 2.4	SE5t
06310−6650.....	HD 46975	NSV	M6 II/III	−0.89	0.87	1.61 ± 0.08	8.2 ± 1.9	SE8t
06534−1647.....	GS CMa	Lb:	M7	−0.11	1.04	1.25 ± 0.09	15.5 ± 2.4	SE5t
06546−2353.....	X CMa	SRb	M5/6 III	−0.96	0.87	1.26 ± 0.04	15.7 ± 0.9	SE5t
06551+0322.....	AZ Mon	M	M9	−0.28	0.64	1.14 ± 0.09	15.6 ± 3.4	SE3t
07034−3551.....	HD 53917	...	M6 III	−2.38	0.89	1.04 ± 0.02	13.2 ± 0.6	SE2t
07091−2902.....	GW CMa	Lb	M5	−0.51	0.73	0.90 ± 0.11	14.1 ± 1.9	SE1t
07118−3438.....	...	...	...	−0.39	1.05	1.53 ± 0.05	12.4 ± 2.6	SE7t
07286−6308.....	V355 Car	L	...	−0.53	0.86	1.16 ± 0.09	7.4 ± 1.7	SE4t
07553−1504.....	...	...	M6	1.14	0.84	1.11 ± 0.27	32.2 ± 5.9	SE3t
08189+0507.....	FZ Hya	Lb	M6	−1.07	0.81	1.16 ± 0.05	5.8 ± 1.0	SE4t
08196+1509.....	Z Cnc	SRb	M6 III	−0.48	0.80	1.37 ± 0.09	22.7 ± 2.6	SE6t
08220−0821.....	FK Hya	Lb	Mb	−2.20	0.89	1.51 ± 0.03	7.4 ± 2.1	SE7t
08286−4728.....	...	...	...	−0.23	0.90	1.00 ± 0.13	12.3 ± 2.2	SE2t
08375−1707.....	AK Hya	SRb	M4 III	−2.08	0.77	1.25 ± 0.05	6.7 ± 1.0	SE4t
08571−5901.....	...	...	...	−0.15	1.07	1.42 ± 0.06	11.9 ± 1.9	SE6t
09076+3110.....	RS Cnc	SRc:	M6 Ib–IIe(S)	−3.07	0.66	1.44 ± 0.02	8.4 ± 0.5	SE6t
09175−5010.....	DM Vel	SRb:	M6	−0.13	0.68	1.00 ± 0.15	10.7 ± 1.9	SE2t
09213−5723.....	...	...	...	−0.65	1.13	1.06 ± 0.04	12.1 ± 2.6	SE3t
09425+3444.....	R LMi	M	M6.5–9.0e(Tc:)	−2.94	0.60	1.20 ± 0.03	5.8 ± 1.1	SE4t
09480−4147.....	SU Vel	SRb	M5 (III)	−1.80	1.00	1.05 ± 0.05	5.5 ± 0.9	SE3t
09511−5356.....	Z Vel	M	M9e	−1.16	0.55	0.90 ± 0.10	6.4 ± 1.5	SE1t
10133−5413.....	W Vel	M	M5–8 IIIe	−1.57	0.62	1.10 ± 0.05	5.8 ± 1.7	SE3t
10147−5057.....	GY Vel	Lb	M4/5 III	−0.18	0.12	0.00 ± 0.00	12.6 ± 2.9	Nt
10176−5802.....	...	...	...	−1.04	1.26	1.29 ± 0.04	17.9 ± 1.7	SE5t
10226−5956.....	CK Car	SRc	M3.5 Iab	−1.51	1.04	1.43 ± 0.02	6.4 ± 1.1	SE6t
10401−5327.....	HH Vel	SRb	M5/6 III	−1.03	1.08	1.42 ± 0.03	6.4 ± 0.9	SE6t
10580−1803.....	R Crt	SRb	M7 III	−3.38	0.77	1.10 ± 0.02	9.4 ± 0.5	SE3t
11125+7524.....	CS Dra	Lb	M5	−1.27	0.90	1.25 ± 0.05	15.4 ± 1.4	SE4t
11153−2152.....	RX Crt	SRb	M3	−0.10	0.20	1.14 ± 0.82	20.5 ± 3.3	Nt

TABLE 1—*Continued*

IRAS PSC	Name	Type of Variable	Spectral Type	[12]	[12] − [25]	F_{11}/F_{12}	F_{13}/F_c	Dust Type
11461−3542.....	HD 102608	...	M7 III	−2.63	1.02	1.17 ± 0.03	9.1 ± 0.8	SE4t
11538+5808.....	Z UMa	SRb	M5 IIIe	−0.89	0.57	0.89 ± 0.27	8.4 ± 1.9	SE1t
12046−0629.....	RW Vir	Lb	M5 III	−1.21	0.61	1.13 ± 0.09	11.5 ± 1.9	SE3t
12277+0441.....	BK Vir	SRb	M7 III	−2.36	0.59	1.15 ± 0.07	4.0 ± 1.0	SE4t
12380+5607.....	Y UMa	SRb	M7 II–III:	−2.08	0.75	1.00 ± 0.05	7.1 ± 0.7	SE2t
13001+0527.....	RT Vir	SRb	M8 III	−3.03	0.78	1.07 ± 0.04	8.5 ± 1.0	SE3t
13022−7650.....	NSV 06083	NSV	...	−0.63	0.91	1.02 ± 0.12	15.2 ± 2.1	SE2t
13114−0232.....	SW Vir	SRb	M7 III	−3.45	0.81	1.12 ± 0.03	9.8 ± 0.9	SE3t
13144−6225.....	V397 Cen	Lb:	M4(S:)	−1.04	1.08	1.20 ± 0.03	7.2 ± 1.3	SE4t
13172+4547.....	V CVn	SRa	M4–6e IIIa:	−1.67	0.77	1.69 ± 0.06	13.0 ± 2.0	SE8t
13269−2301.....	R Hya	M	M6–9eS(Tc)	−4.37	0.48	0.98 ± 0.10	6.7 ± 0.4	SE2t
13342−5321.....	CE Cen	M:	...	−0.16	0.77	1.30 ± 0.13	20.6 ± 4.3	SE5t
13466−3512.....	...	...	...	0.47	1.31	1.66 ± 0.22	39.3 ± 4.8	SE8t
13586−4617.....	...	...	...	−0.36	1.02	1.16 ± 0.05	16.9 ± 1.3	SE4t
14003−7633.....	θ Aps	SRb	M7 III	−3.54	0.72	1.27 ± 0.03	6.5 ± 0.5	SE5t
14086−2839.....	RU Hya	M	M6–8.8e	−1.09	0.82	1.52 ± 0.08	11.4 ± 2.2	SE7t
14167−6717.....	UZ Cir	M	Me	−0.03	0.77	1.06 ± 0.12	14.4 ± 3.0	SE3t
14180−7107.....	...	...	...	−0.48	1.07	1.41 ± 0.13	16.5 ± 3.4	SE6t
14219+2555.....	RX Boo	SRb	M6.5–8 IIIe	−3.69	0.80	1.07 ± 0.03	12.1 ± 0.8	SE3t
14280−2952.....	Y Cen	SRb:	M4–7e	−1.84	0.60	0.92 ± 0.10	7.2 ± 0.9	SE1t
14281−6318.....	...	...	...	0.05	0.81	1.21 ± 0.07	13.6 ± 2.2	SE4t
14371+3245.....	RV Boo	SRb	M5–7e	−1.61	0.93	1.26 ± 0.05	8.2 ± 1.7	SE5t
14598−7124.....	V Aps	Lb	Mb	−0.40	0.97	1.15 ± 0.07	13.4 ± 1.7	SE3t
15223−0203.....	HD 137227	...	M7	−1.38	1.10	1.39 ± 0.04	8.4 ± 1.1	SE6t
15298+0348.....	WW Ser	M	M8e	−0.49	0.65	0.95 ± 0.11	9.2 ± 2.0	SE1t
15314+7847.....	S UMi	M	M6–9e	−1.78	0.58	1.08 ± 0.05	5.6 ± 0.7	SE3t
15380−6545.....	IZ TrA	Lb	M6 III	−0.80	0.66	0.92 ± 0.08	5.8 ± 1.1	SE1t
15566+3609.....	RS CrB	SRa	M7	−0.67	0.87	1.41 ± 0.04	15.1 ± 2.0	SE6t
16011+4722.....	X Her	SRb	M6–8e	−3.08	0.80	1.40 ± 0.02	8.4 ± 0.7	SE6t
16063−4906.....	V Nor	SRb	M5 III	−0.75	0.36	0.76 ± 0.43	9.9 ± 2.3	SE1t
16205−4830.....	...	...	...	−0.41	0.86	1.34 ± 0.07	17.5 ± 3.6	SE5t
16269+4159.....	g Her	SRb	M6 III	−2.97	0.39	0.78 ± 0.21	4.8 ± 0.5	SE1t
16306+7223.....	R UMi	SRb	M7 IIIe	−1.43	0.64	1.01 ± 0.08	10.7 ± 0.7	SE2t
16351−5448.....	...	...	...	−0.03	0.99	1.20 ± 0.05	9.9 ± 1.4	SE4t
16383−1952.....	IRC −20324	...	M7	−0.43	0.81	1.07 ± 0.07	13.8 ± 1.2	SE3t
16387−2700.....	AX Sco	SRb	M5 III	−0.56	0.63	1.12 ± 0.09	11.0 ± 1.6	SE3t
16390−4354.....	...	...	...	−0.18	0.80	1.29 ± 0.09	15.0 ± 2.2	SE5t
16418+5459.....	S Dra	SRb	M6 III:	−1.66	0.93	1.34 ± 0.03	5.8 ± 0.9	SE5t
16534−3030.....	RR Sco	M	M6–9 II–IIIe	−2.06	0.49	1.06 ± 0.08	5.1 ± 0.9	SE3t
17079−7405.....	W Aps	Lb	M6	−0.58	0.94	1.13 ± 0.07	8.3 ± 1.6	SE3t
17080−3215.....	AH Sco	SRc	M4–5 Ia–Iab	−3.37	0.92	1.33 ± 0.02	7.0 ± 1.2	SE5t
17081+6422.....	TV Dra	Lb	M8p(S)	−0.82	0.65	0.92 ± 0.11	4.7 ± 0.9	SE1t
17123+1107.....	V438 Oph	SRb	M0–7e	−0.84	0.65	0.90 ± 0.13	5.5 ± 0.8	SE1t
17213−2219.....	IRC −20359	...	M6	−0.34	1.18	1.17 ± 0.10	22.1 ± 2.5	SE4t
17343+1052.....	V790 Oph	M	M5 IIIe	−0.31	0.66	1.47 ± 0.11	16.6 ± 2.6	SE7t
17349−3039.....	...	...	...	−0.29	1.17	1.37 ± 0.06	17.2 ± 2.9	SE6t
17361+5746.....	TY Dra	Lb	M5–8	−0.92	1.16	1.59 ± 0.02	9.5 ± 1.1	SE8t
17508−3419.....	BN Sco	M	M6	−0.74	0.91	1.19 ± 0.09	8.8 ± 1.6	SE4t
17531−4947.....	W Ara	SRb	M5 III	−0.10	0.83	0.95 ± 0.19	11.6 ± 2.8	SE1t
17538−3118.....	V749? Sco	M:?	M6?	−0.29	0.86	1.29 ± 0.06	9.4 ± 1.9	SE5t
17541+1110.....	RT Oph	M	M7e(C)	−0.80	0.71	1.09 ± 0.07	9.4 ± 1.4	SE3t
18009−4001.....	...	...	...	−0.31	0.92	1.43 ± 0.10	14.1 ± 2.7	SE6t
18044−2927.....	AFGL 2069	...	...	−1.05	1.16	1.43 ± 0.04	7.2 ± 1.4	SE6t
18155−1036.....	...	...	...	−0.17	0.63	1.22 ± 0.16	24.8 ± 5.0	SE4t
18186+3143.....	TU Lyr	Lb	M6	−0.92	0.92	1.16 ± 0.06	10.5 ± 1.4	SE4t
18222+3933.....	TW Lyr	M	M6	−0.55	0.67	0.93 ± 0.05	11.9 ± 1.1	SE1t
18243+0352.....	V988 Oph	SRb	M7e	−1.11	0.80	1.57 ± 0.06	12.1 ± 2.0	SE8t
18309−6955.....	RT Pav	SRb	M4/5 III	−0.50	0.95	1.38 ± 0.09	14.2 ± 2.4	SE6t
18401+2854.....	FI Lyr	SRb	M1	−1.30	0.98	1.01 ± 0.05	8.8 ± 2.4	SE2t
18432+1343.....	...	...	...	0.67	1.23	1.30 ± 0.11	23.8 ± 4.5	SE5t
19007−2247.....	SU Sgr	SRb	M6 III	−1.59	0.69	1.19 ± 0.07	5.4 ± 0.9	SE4t
19055+0613.....	V347 Aql	Lb	M6–8	−1.37	0.57	0.92 ± 0.06	12.4 ± 0.8	SE1t
19143−5032.....	V Tel	SRb	M6/8	−1.48	0.97	1.04 ± 0.04	5.1 ± 1.4	SE2t
19152−3640.....	V924 Sgr	M	Me	−0.59	1.04	1.49 ± 0.04	10.5 ± 1.5	SE7t
19194+1734.....	T Sge	SRb	M4–6.5	−1.74	0.74	1.05 ± 0.03	4.2 ± 1.3	SE3t
19243+7135.....	YZ Dra	M	M8e	−0.59	0.69	1.29 ± 0.06	7.7 ± 1.8	SE5t
19247−1722.....	IRC −20563	...	M8	−1.25	0.95	1.16 ± 0.04	12.3 ± 2.0	SE4t
19287+4602.....	AF Cyg	SRb	M5–7e	−1.10	0.68	1.06 ± 0.13	6.8 ± 1.4	SE3t
19296+4331.....	UV Cyg	SRb	M6–8	−1.41	0.94	1.25 ± 0.03	11.4 ± 1.1	SE4t
19328+3039.....	IRC +30375	NSV	M7	−0.73	0.57	1.12 ± 0.07	6.6 ± 1.5	SE3t
19369+2823.....	BG Cyg	M	M7–8e	−0.74	0.50	0.97 ± 0.16	5.2 ± 1.2	SE2t
19503+2219.....	NS Vul	Lb:	M5 III	−2.26	0.80	1.33 ± 0.03	6.2 ± 0.8	SE5t

TABLE 1—*Continued*

IRAS PSC	Name	Type of Variable	Spectral Type	[12]	[12] − [25]	F_{11}/F_{12}	F_{13}/F_c	Dust Type
19510−5919.....	S Pav	SRa	M7–8 II–IIIe	−3.12	0.58	0.97 ± 0.09	7.0 ± 0.9	SE2t
20010+3011.....	V718 Cyg	SRb	M0–5	−0.78	1.19	1.23 ± 0.04	6.4 ± 1.3	SE4t
20038−2722.....	V1943 Sgr	Lb	M8	−2.86	0.53	1.00 ± 0.09	6.7 ± 0.7	SE2t
20047+1248.....	SY Aql	M	M5–7e	−0.90	0.81	1.50 ± 0.08	8.9 ± 2.2	SE7t
20075−6005.....	X Pav	SRb	Mc	−3.23	0.79	1.15 ± 0.02	10.8 ± 1.1	SE3t
20079−0146.....	V584 Aql	Lb	M8	−0.82	0.76	1.13 ± 0.11	12.9 ± 1.8	SE3t
20113+4917.....	AC Cyg	SRb	M7	−1.37	0.89	1.41 ± 0.09	14.0 ± 2.0	SE6t
20193+3527.....	V1749 Cyg	Lc	M3 Iab	−0.42	1.11	1.13 ± 0.07	12.4 ± 1.9	SE3t
20198+4017.....	V405 Cyg	Lb	M6.5	−0.34	0.75	1.23 ± 0.15	14.1 ± 2.6	SE4t
20248−2825.....	T Mic	SRb	M7 IIIe	−3.10	0.53	0.94 ± 0.08	6.4 ± 1.1	SE1t
20248+7505.....	UU Dra	SRb	M8 IIIe	−1.67	1.14	1.20 ± 0.02	9.4 ± 1.6	SE4t
20255+3712.....	...	...	...	−2.15	4.28	0.94 ± 0.09	8.8 ± 0.7	SE1t
20359−3806.....	AFGL 5589	NSV	...	−1.17	0.75	1.14 ± 0.09	7.4 ± 1.6	SE3t
20392+1141.....	Y Del	M	M8e	−0.29	1.01	1.18 ± 0.06	9.9 ± 2.0	SE4t
20431+1754.....	U Del	SRb	M5 II–III	−1.75	0.91	1.29 ± 0.05	6.2 ± 1.1	SE5t
20479+0554.....	DO 7021	...	M5	−0.36	1.00	1.16 ± 0.10	9.4 ± 2.2	SE4t
20502+4709.....	RZ Cyg	SRa	M7.0–8.2ea	−1.42	0.99	1.12 ± 0.03	10.4 ± 0.8	SE3t
20507+2310.....	RX Vul	M	M9e	−1.01	0.73	1.00 ± 0.06	13.4 ± 1.2	SE2t
20511+2523.....	IN Vul	Lb	M7	−0.21	0.83	0.99 ± 0.12	14.6 ± 1.6	SE2t
20529+3013.....	UX Cyg	M	M4–6.5e	−1.96	0.99	1.56 ± 0.03	5.9 ± 1.6	SE8t
21028+2711.....	NSV 13514	NSV	M7	−0.13	0.99	1.20 ± 0.07	15.4 ± 2.6	SE4t
21044−1637.....	RS Cap	SRb	M4	−2.27	0.80	1.53 ± 0.03	6.3 ± 1.9	SE7t
21245+6221.....	SW Cep	SRc	M3.5 Ia–Iab	−1.10	1.25	1.43 ± 0.03	6.9 ± 1.3	SE6t
21260+5931.....	HR 8224	NSV	M3 II–III	0.42	0.15	0.00 ± 0.00	17.2 ± 3.3	Nt
21377−0200.....	HT Aqr	var	M5	−0.83	0.92	1.06 ± 0.07	7.0 ± 1.1	SE3t
21389+5405.....	RU Cyg	SRa	M6–8e	−2.07	0.92	1.32 ± 0.03	7.2 ± 0.7	SE5t
21439−0226.....	EP Aqr	SRb	M8 III	−3.38	0.81	1.28 ± 0.03	11.0 ± 1.3	SE5t
21543−1421.....	HD 208519	NSV	M7 III	−1.06	1.06	1.15 ± 0.05	10.8 ± 1.0	SE3t
22017+2806.....	TW Peg	SRb	M6–M8 III	−2.42	0.97	1.43 ± 0.02	7.1 ± 0.8	SE6t
22035+3506.....	SV Peg	SRb	M7 III	−2.43	0.92	1.10 ± 0.03	11.9 ± 0.6	SE3t
22097+5647.....	CU Cep	SRb	M4–6	−2.14	1.12	1.42 ± 0.02	5.6 ± 1.7	SE6t
22142−8454.....	BW Oct	Lb:	M7 III	−1.76	0.82	1.26 ± 0.02	5.7 ± 0.6	SE5t
22315+2418.....	SS Peg	M	M6–7e	−1.20	0.35	0.95 ± 0.14	10.1 ± 1.7	SE2t
22359−1417.....	AB Aqr	Lb	M7	−0.35	0.85	0.95 ± 0.13	12.8 ± 1.6	SE2t
22525−2952.....	V PsA	SRb	Mb	−2.35	0.69	1.24 ± 0.05	6.6 ± 0.8	SE4t
22553+1744.....	BI Peg	SRa	M6–9e	0.18	0.90	1.45 ± 0.16	22.6 ± 4.5	SE7t
22594+6117.....	V352 Cep	Lb	M7:	−0.16	1.13	1.92 ± 0.28	15.9 ± 3.5	SE8t
23000+5932.....	AS Cep	Lb	M3	−0.73	1.16	1.34 ± 0.03	7.5 ± 1.6	SE5t
23013+3735.....	CF And	Lb	M7	−1.46	0.93	1.38 ± 0.07	19.8 ± 2.0	SE6t
23173+4823.....	BE And	SRb	M5	−0.26	0.47	1.09 ± 0.17	12.0 ± 2.3	SE3t
23180+0838.....	S Peg	M	M5–8.5e	−0.37	0.45	0.93 ± 0.27	15.8 ± 3.0	SE1t
23281+5742.....	V358 Cas	Lc	M3Ia-Iab	−1.18	1.36	1.42 ± 0.04	9.4 ± 2.0	SE6t
23528+4821.....	RS And	SRa	M7–10	−1.59	0.70	1.30 ± 0.07	11.2 ± 1.2	SE5t
23558+5106.....	R Cas	M	M6–10e	−4.19	0.60	1.27 ± 0.03	4.1 ± 1.3	SE5t

Table 1. Paper I defines the *IRAS* color [12] − [25] and the flux ratio F_{11}/F_{12}. The ratio F_{13}/F_c measures the integrated strength of the 13 μm emission feature relative to the underlying continuum. The dust types are also defined in Paper I, but here we have added the "t" designation for 13 μm sources. A dust type of N denotes a naked star with no excess dust emission.

3. GROUND-BASED CONFIRMATION

The 13 μm feature occurs uncomfortably close to the region in which the spectra from the blue and red detectors of the LRS are spliced together. Because any problems normalizing the two spectra to each other might produce spurious spectral components in the 12–14 μm regime, ground-based confirmation of the 13 μm feature would help to bolster confidence that the feature is real.

In Figure 2, we present spectra of four bright 13 μm sources obtained with GLADYS, the Air Force Geophysics Laboratory long-slit 10 μm spectrometer, at the 2.3 m telescope of the Wyoming Infrared Observatory in 1991 and 1993. Sloan, Grasdalen, & LeVan (1993) and references therein describe the instrument and observing methods. We obtained spectra of each source by summing spectra from individual rows on the array and then co-adding the resultant one-dimensional spectra. To correct for transmission, we divided program spectra by spectra of standard stars taken at similar air masses and then multiplied by the assumed spectrum for the standard. For α Boo and β Peg, we used the spectral templates calibrated by Cohen et al. (1995) and regridded to the GLADYS wavelength scale. For β And, we regridded the LRS spectrum after making the corrections described by Cohen, Walker, & Witteborn (1992). Details of the observations can be found in Table 2. Figure 2 shows that we have confirmed the 13 μm feature in all of these sources.

TABLE 2

GLADYS Observation Log

Source	*IRAS* Designation	Date (UT)	Standard
HD 11979.....	01556+4551	1993 Jun 30	β And
RX Boo	14219+2555	1991 Feb 7, 1993 Mar 1	α Boo
X Her	16011+4722	1991 Feb 7	α Boo
R Cas	23558+5106	1993 Jun 30	β Peg

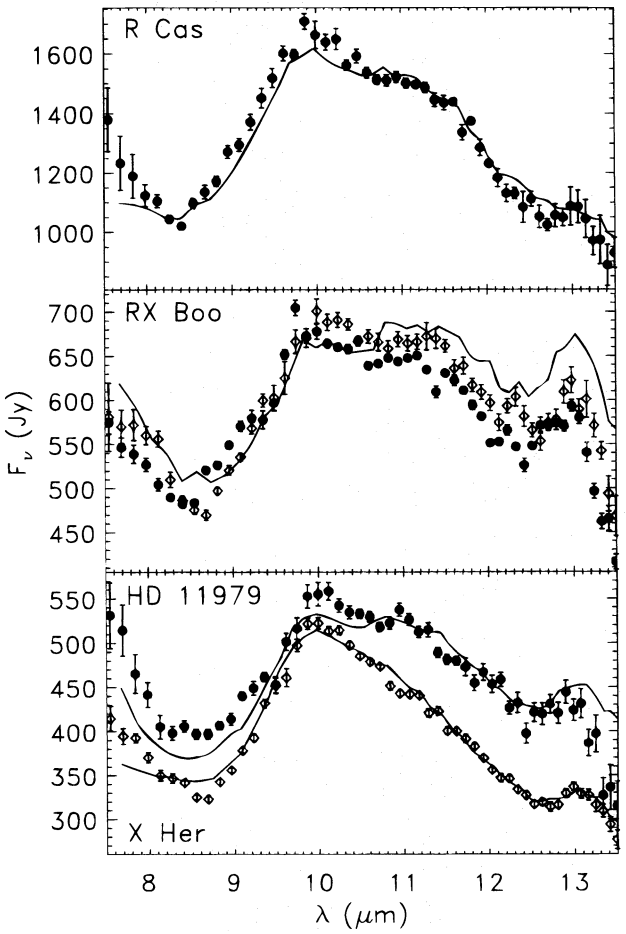

FIG. 2.—Sample ground-based confirmation of 13 μm emission. In all panels, the error bars depict GLADYS observations, and the curves depict LRS data. *Top*: R Cas. The LRS spectrum has been multiplied by 0.87. *Middle*: RX Boo as observed in 1991 (*open diamonds*) and 1993 (*filled circles*). The LRS spectrum has been multiplied by 0.8. *Bottom*: HD 11979 (*filled circles*) and X Her (*open diamonds*). The LRS spectra have been multiplied by 1.1 and 0.85, respectively.

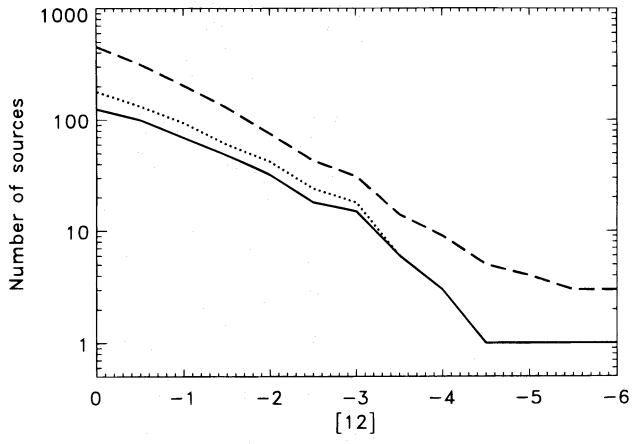

FIG. 3.—Completeness diagrams for the total AGB sample defined in Paper I (*dashed line*), the total sample of 13 μm sources (*dotted line*), and the smaller sample of 13 μm sources from the AGB sample (*solid line*). At each magnitude, we plot the number of sources brighter than that magnitude. From [12] = −6.0 to −3.0, the fraction of 13 μm sources among the AGB sources increases as the sample size becomes statistically significant. Beyond this magnitude, the fraction of 13 μm sources decreases because of the difficulty of detecting 13 μm features in noisier spectra.

4. COMPLETENESS OF THE SAMPLE

We wish to exclude spurious 13 μm sources from our sample, even at the risk of excluding real sources with noisy spectra. As a result, the criteria described in § 2 are very conservative and will select against noisy or faint spectra or weak 13 μm features. Figure 3 illustrates this effect by plotting the completeness of the AGB sample from Paper I and the sample of 13 μm sources discussed here. For sources fainter than [12] = −2.0 ($F_{12} < 180$ Jy), we are clearly missing some 13 μm sources, and the percentage of missing 13 μm sources increases as the sources get fainter. We estimate that our sample of 13 μm sources is reasonably complete only for sources brighter than [12] = −3.0 ($F_{12} >$ 440 Jy) (i.e., 15 of 31 AGB sources).

The AGB sample includes only those sources that have been optically identified as variables and therefore selects against heavily obscured sources. Most of the 13 μm sources come from the AGB sample, but 59 do not. Many of these sources are not optically identified as variables because they are hidden beneath thicker, redder shells (in fact some have no identified optical counterpart). As a consequence, when we make our comparisons with the AGB sample, we will generally examine only those 13 μm sources that come from the AGB sample and compare them only to the dusty sources in the AGB sample.

5. PROPERTIES OF THE 13 MICRON SOURCES

5.1. *Optical Variability*

We have variability types for 78% of the 13 μm sources (Fig. 4). Of these, 22% are Mira variables, 22% are irregulars, and over half (55%) are semiregular variables. Figure 5 plots the number of each variability type against their 12 μm magnitudes and shows clearly the effects of incompleteness of the different variability types. Of the 10 brightest SRbs associated with oxygen-rich dust emission in the LRS database, *all show a 13 μm feature!* At [12] = −2.0, where the completeness of our 13 μm sample becomes questionable, over three-quarters of the SRb variables (86 of 126) still show 13 μm emission by our conservative standards, so we estimate that ∼75%–90% of the SRb variables are 13 μm sources. Correcting for incompleteness, we estimate that only ∼20%–25% of the Miras are 13 μm sources, a much smaller percentage than for SRb variables. Despite the poor

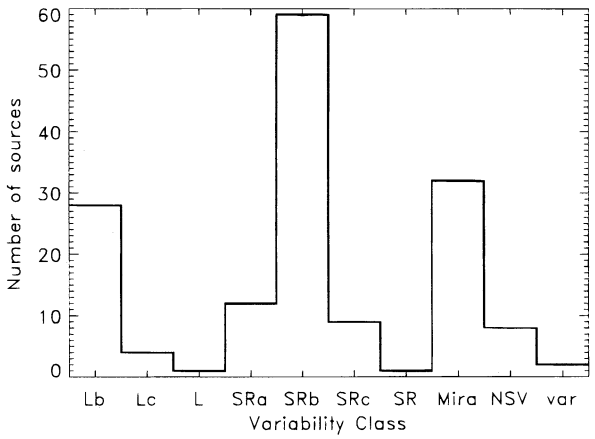

FIG. 4.—Distribution of variability class among the total 13 μm sample. NSV means new suspected variable. Of the 156 known or suspected variables, 59, or 38%, are positively identified as SRb variables.

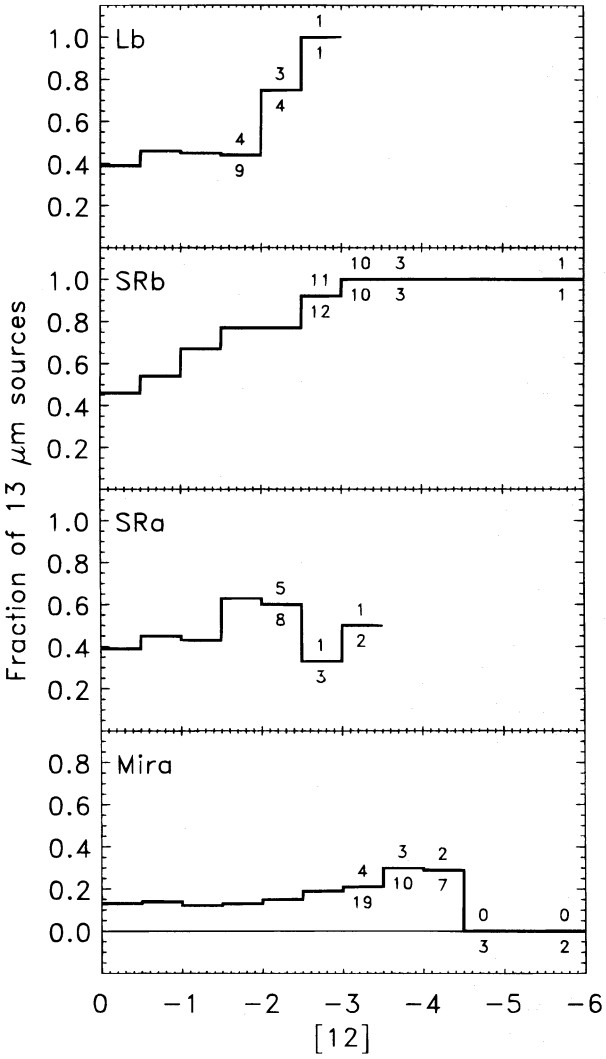

FIG. 5.—Fraction of 13 μm sources from each variability class in the AGB sample, plotted against limiting magnitude to illustrate the bias against detecting 13 μm features in fainter spectra. To illustrate how few sources are represented in the ratios for bright magnitudes, we have given the number of 13 μm sources (above the curve) and the number of AGB sources (below the curve). For example, for Miras brighter than −3.0, four of 19 show 13 μm emission. A very large fraction of the SRb variables, easily over 75% of the brighter sources, show 13 μm emission. A much smaller fraction of Miras exhibit emission at 13 μm, roughly 20%–25% of the brighter sources. Small sample sizes make an analysis of Lb and SRa variables more difficult. At [12] = −1.5, about 45% of the Lb variables and over 60% of the SRa variables emit at 13 μm. Whatever the exact percentage, the percentage of 13 μm sources is intermediate in these two classes between SRb and Mira variables.

statistics for Lb and SRa variables, we estimate that ~50%–60% of both types are 13 μm sources, a percentage intermediate between the Mira and SRb variables. If we apply these estimated percentages to the entire AGB sample, we can expect that approximately 40%-50% of all AGB sources associated with oxygen-rich circumstellar dust possess 13 μm features!

When we investigate the period distributions between the Mira and SRb variables, we find that the 13 μm sources appear to have identical periodicities to the parent AGB populations. The mean period of SRb variables is 194 days, and for the Miras, it is 393 days.

5.2. *Galactic Distribution and Radial Velocity*

The 13 μm feature probably arises from a different type of dust than the amorphous silicates usually associated with the 10 μm feature. If this difference in dust chemistry results from an unusual stellar chemistry or different progenitor mass, then the 13 μm emission feature may be isolated to a particular population component of the Galaxy. We therefore investigate the distribution of 13 μm sources with Galactic latitude and longitude and radial velocity (Table 3, Fig. 6).

In general, the Galactic and radial velocity distribution of the 13 μm sources follows the parent AGB sample fairly closely, with some minor differences. The 13 μm sources show a slightly higher mean absolute latitude (23°.8) than the AGB sample (22°.0) (Table 3). We attribute this small difference to the difficulty in detecting 13 μm emission in fainter spectra. Fainter sources will generally be at greater distances and thus be at lower Galactic latitudes, so their exclusion increases the mean apparent latitude of our 13 μm sample. The additional 13 μm sources tend to lie at lower Galactic latitudes, as expected for more heavily obscured infrared sources (e.g., Jura & Kleinmann 1989, 1992b; Jura, Yamamoto, & Kleinmann 1993). Including them in our 13 μm sample drops the mean Galactic latitude to 20°.7.

Figure 6 shows that both the AGB sample and its subset of 13 μm sources are slightly concentrated toward the first quadrant (longitudes of 0°–90°). Including all of the 13 μm sources enhances the number of 13 μm sources in the half of the sky toward the Galactic center. Jura & Kleinmann (1992a, b) observe a slightly greater percentage of AGB stars in the hemisphere facing the Galactic center, which can be attributed to a radial exponential density gradient of these stars (Habing 1988). We suspect that the slightly greater percentage of SRb variables in the anticenter (±30°) detected by Kerschbaum & Hron (1992) results from statistical fluctuations in their data.

As can be seen from Table 3, the absolute magnitudes of the radial velocities (using data obtained from the SIMBAD database) for the 13 μm sources are very similar to the parent population.

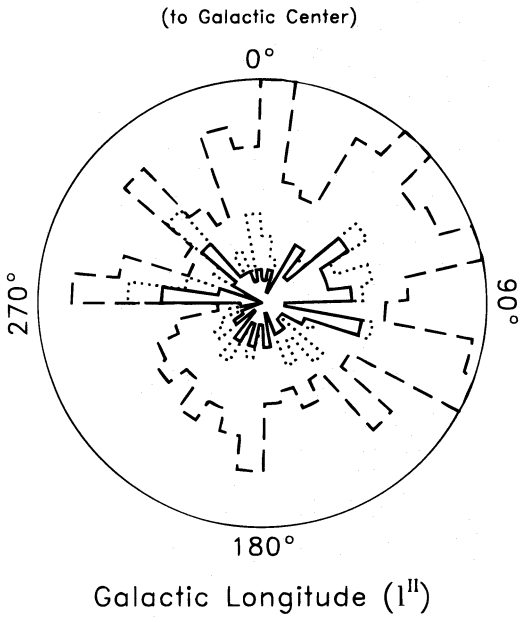

FIG. 6.—Distribution with Galactic longitude, plotted as a polar histogram. The radius at each angle is proportional to the number of sources in that direction. The lines are as defined in Fig. 3. All three samples show an enhancement in the first quadrant, between Galactic longitudes of 0° and 90°.

TABLE 3

POPULATION PROPERTIES

	Galactic Latitude				Radial Velocity (km s^{-1})			
	AGB		13 μm		AGB		13 μm	
Class	n	$\langle \lvert b^{II} \rvert \rangle$	n	$\langle \lvert b^{II} \rvert \rangle$	n	$\langle \lvert v_{rad} \rvert \rangle$	n	$\langle \lvert v_{rad} \rvert \rangle$
Lb	67	19°.4	28	20°.2	4	35°.8	2	32°.8
SRb.....	126	26.0	59	26.5	86	26.5	38	22.3
SRa.....	28	21.6	11	25.1	14	28.7	7	33.5
Mira.....	232	20.7	30	21.4	117	30.1	17	24.7
Total.....	453	22.0	128	23.8	221	28.7	64	24.5

When we examine the subset of 13 μm sources from the larger AGB sample, we conclude that the Galactic latitude, Galactic longitude, and radial velocities indicate that the subset of 13 μm sources comes from the same population of stars as the AGB stars. The Galactic coordinates and radial velocities of the additional 13 μm sources differ slightly from the AGB sample, a result consistent with the different selection effects determining the samples.

5.3. *Optical Spectral Class*

A comparison of the optical spectral classes of the AGB sample with the subset of 13 μm sources (Table 4) reveals a slight but noticeable difference. The 13 μm sources tend to be slightly cooler than the parent population. This effect is small, but it occurs in all four variability classes. For Lb variables, the difference in spectral class corresponds to a temperature difference of ~50 K, while for SRa variables, the difference is nearly one subclass (~100 K). But these samples are small. The larger samples of Mira and SRb variables show much smaller differences that correspond to only ~10 K, so we question the significance of these differences. The temperature difference is not apparent when we compare the total samples because the number of cool Miras dominates the AGB sample but represents a much smaller fraction of the 13 μm sources.

5.4. *Infrared Properties*

Table 5 compares the infrared properties of the sample of 13 μm sources with the larger AGB sample. The dust emission contrast was defined in Paper I as the ratio of the dust to stellar emission between 7.67 and 14.03 μm. As shown in Table 5, including the additional 13 μm sources increases the dust contrast and redness of the sample because these sources tend to be more obscured. When we compare the AGB sample only to the 13 μm sources from that sample, the difference in [12] − [25] color vanishes, and the difference in dust contrast almost vanishes.

TABLE 4

MEAN OPTICAL SPECTRAL CLASS

	⟨Optical Spectral Class⟩	
Class	AGB	13 μm
Lb	5.7 ± 1.9	6.2 ± 1.4
SRb.....	5.8 ± 1.2	5.9 ± 1.2
SRa.....	6.1 ± 1.8	7.0 ± 1.2
Mira.....	7.1 ± 1.3	7.2 ± 1.2
Total.....	6.5 ± 1.5	6.4 ± 1.3

The distribution of the 13 μm sources with SE index follows the parent AGB sample fairly closely, as shown in Figure 7. If the 13 μm feature were limited to the three-component class of LML, we would expect 13 μm emission to cluster where the three-component class clusters: SE indices of 3–4. When we include the additional 13 μm sources, the emission does concentrate in SE indices of 3–5, but significant numbers of 13 μm sources have emission outside this range, either broad or classic silicate emission. Figure 8 reinforces this point by illustrating sample dust

TABLE 5

INFRARED PROPERTIES

Class	n	[12] − [25]	Dust Emission Contrast	SE Index
Lb	67	0.86 ± 0.24	0.62 ± 0.58	4.6 ± 2.4
SRb.....	126	0.76 ± 0.20	0.38 ± 0.27	4.3 ± 2.3
SRa.....	28	0.76 ± 0.28	0.51 ± 0.37	4.4 ± 3.0
Mira.....	232	0.73 ± 0.22	0.61 ± 0.36	4.6 ± 2.0
All AGB	453	0.76 ± 0.22	0.54 ± 0.39	4.5 ± 2.3
AGB 13 μm.....	128	0.76 ± 0.21	0.50 ± 0.36	4.1 ± 2.4
All 13 μm	187	0.83 ± 0.35	0.61 ± 0.45	4.3 ± 2.4

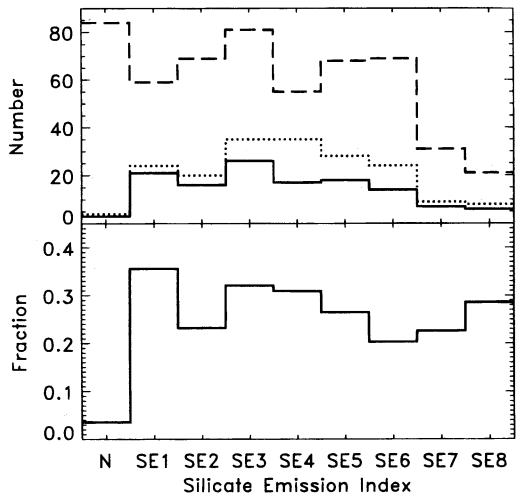

FIG. 7.—Distribution with SE index. The top panel plots the number of sources in the AGB sample (*dashed line*), 13 μm sources from the AGB sample (*solid line*), and total 13 μm sample (*dotted line*). The bottom panel shows how the fraction of 13 μm sources within the AGB sample decreases slightly as the SE index increases. Note that the additional 13 μm sources are slightly more concentrated in SE3–4 than the AGB 13 μm sources.

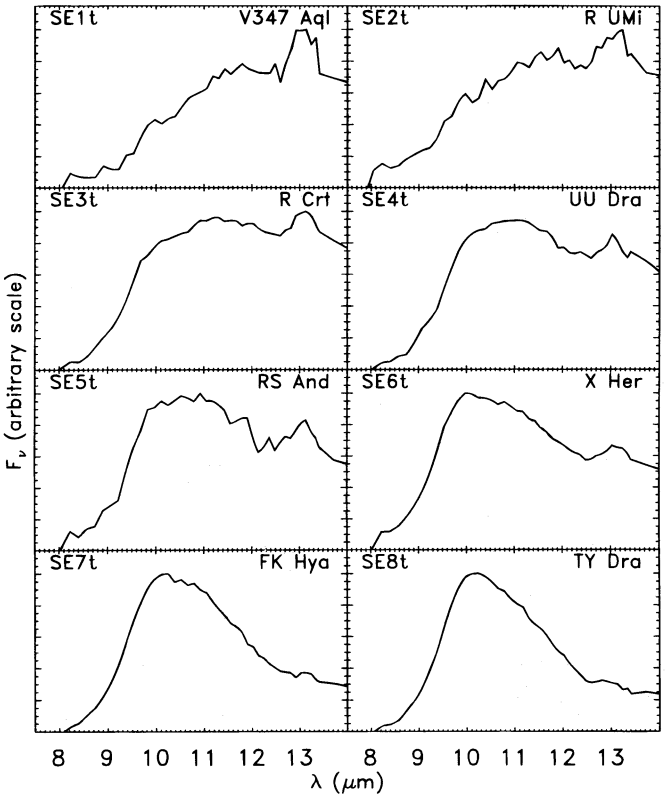

FIG. 8.—Examples of 13 μm features associated with dust spectra of each SE index, from broad emission (SE1) to classic narrow emission (SE8). In each of these, the stellar contribution to the spectrum has been removed. This figure is analogous to Fig. 3 in Paper I.

spectra with 13 μm features for each SE index. We conclude (as in Paper I) that the carrier of the 13 μm feature is associated with all known types of oxygen-rich circumstellar dust.

The primary effect selecting against the detection of 13 μm emission is a poor signal-to-noise ratio (S/N) in the dust spectrum. Sources with thinner shells will have spectra with lower dust emission contrasts. Lower contrasts imply a lower S/N in the dust, which makes these sources less likely to be detected as 13 μm sources. As previously noticed (Vardya et al. 1986; Onaka et al. 1989; Paper I), broad emission spectra (SE1–2) tend to have lower contrasts, so we believe we are selecting against 13 μm emission in lower SE indices. Despite this selection effect, there is a noticeable tendency for broader dust profiles to be associated with 13 μm features. AGB sources with SE indices of 1–4 are more likely to be 13 μm sources (30%) compared to SE5–8 (24%). Without the selection effect, this difference would be even greater. The typical 13 μm source would show a bluer [12] − [25] color, have a lower dust emission contrast, and have a lower SE index than our results suggest.

6. DISCUSSION

Of the sample of 546 AGB sources defined in Paper I, 24% show an emission feature at 13 μm. If we limit our sample to those AGB sources showing emission from oxygen-rich dust, this percentage rises to 28%. From our analysis of the completeness of 13 μm sources, we estimate that actually 40%–50% of all AGB sources with circumstellar shells of oxygen-rich dust have 13 μm features. We note that our sample of 13 μm sources also includes some Lc and SRc variables, which are associated with supergiants, in addition to AGB sources.

The Galactic distribution and radial velocities of our 13 μm sample follow the parent AGB sample, and we have seen 13 μm emission associated with all known types of emission spectra from oxygen-rich dust. The infrared colors and shell contrasts also do not point to any peculiarities in the 13 μm sources. All of this evidence suggests that 13 μm emission occurs commonly in oxygen-rich dust shells.

Of the many properties of AGB variables and 13 μm sources considered here, the overwhelming correlation is that all or most of the SRb variables show 13 μm emission. Mira variables (few of which show 13 μm emission) pulsate very strongly and regularly, producing well-defined shock fronts that propagate through the stellar atmosphere. These shocks result in the well-known hydrogen emission spectra so often used to identify Miras. Semiregular variables do not pulsate as strongly and show hydrogen in emission much less frequently, perhaps because they are pulsating in an overtone mode and not in the fundamental like Miras (Jura & Kleinmann 1992b; Kerschbaum & Hron 1992).

Tielens (1989) has emphasized that the physical conditions within the dust formation zone determine the composition and structure of grains forming in stellar outflows. In Mira variables, a clear relation exists between the asymmetry of the visual light curve and the spectra produced by the dust in the infrared (Vardya et al. 1986). Miras with symmetric light curves tend to exhibit the broad emission component (SE1–2), while Miras with increasingly asymmetric light curves show increasingly narrow emission, looking more and more like the classic silicate feature (SE8). This suggests that the physical conditions within the dust formation zone depend on how the shocks from the stellar atmosphere interact with the outflows. Perhaps the absence or weakness of these shocks in semiregulars allows the carrier of the 13 μm feature to form and survive.

The relation between the formation of dust in evolved stars and stellar pulsation has long been suspected (e.g., Iben & Renzini 1983; Habing 1990). As Table 5 shows, the dust emission contrasts of the SRb variables tend to be lower than for the other AGB variables (by roughly half a standard deviation, and this despite the similarity of [12] − [25] colors). The reason the SRb variables show a higher fraction of 13 μm sources may be related to the reduced amount of dust emission seen in these sources. Overtone pulsations may result in less mass loss, which in turn may result in the formation of unusual types of dust.

Little-Marenin & Little (1988), in their investigation of the infrared spectra of S and MS stars, suggested that the 13 μm feature may identify a source as an S star precursor. Our sample of 13 μm sources does not contain an abnormal number of MS or S stars, and thus it provides no support for this hypothesis. However, the weak ZrO bands used to identify MS stars are easily missed. Many of our spectral classifications are dated (they are primarily from the GCVS), so we cannot rule out the possibility that 13 μm emission may occur more frequently in MS stars. A careful examination of optical spectra from 13 μm sources would settle the matter.

Glaccum (1995) has suggested that the 13 μm feature may arise from sapphire, but little published evidence to support this hypothesis exists. Sapphires and rubies are both forms of α-Al_2O_3, or corundum, a crystalline alumina material. Figure 9 compares the sum of the 13 μm features in all SRb variables in our sample to the optical efficiency of α-Al_2O_3, as determined from band positions, strengths, and widths

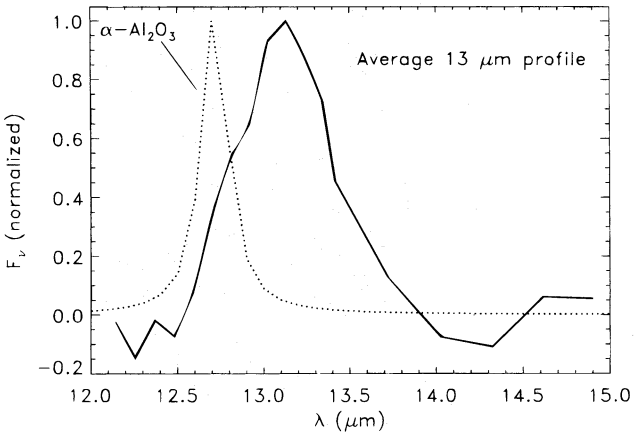

FIG. 9.—Comparison of the 13 μm emission feature (*solid line*) to the optical efficiency of the α-Al_2O_3 feature (*dotted line*; Toon et al. 1976). The 13 μm feature is the sum of the residual in all SRb spectra after fitting and removing a polynomial to the spectrum over the wavelength ranges 10.66–12.59 μm and 13.72–15.18 μm. The observed feature peaks at 13.1 μm and has a FWHM of 0.5 μm. The α-alumina feature is displaced to 12.7 μm and is substantially narrower (FWHM 0.2 μm). The 13 μm feature clearly does not arise from a material identical to the ground-based sample, but it may arise from a related material.

measured by Toon, Pollack, & Khare (1976). While this figure does not rule out a relation, the differences in wavelength and FWHM are substantial. Further theoretical investigation and laboratory measurement might help determine whether or not corundum is related to the carrier of the 13 μm feature.

7. SUMMARY

We have searched the LRS database for sources with 13 μm emission features and have found 187 such sources. Because of the difficulties in detecting this weak feature in spectra from faint sources, we believe our sample to be very incomplete. While we have found 13 μm features in only 28% of the AGB sources with oxygen-rich dust, we estimate that the true percentage is closer to 40%–50%. In particular, about 75%–90% of the SRbs with oxygen-rich dust show 13 μm features.

The strong tendency of SRb variables to be associated with 13 μm emission provides a clue about how the carrier may form. The pulsations in these sources are not as well-ordered or as strong as in Mira or SRa variables, and SRb variables with dust emission tend to show weaker emission than other dusty AGB variables.

Other than the strong tendency of SRb variables to show 13 μm emission, we see no peculiarities among the 13 μm sources. Their distribution in the Galaxy, their radial velocities, their infrared colors, and the contrasts of their shells in the infrared all follow the parent population. The association of 13 μm emission with all known types of emission from oxygen-rich dust suggests that the carrier of the 13 μm emission feature occurs commonly in circumstellar dust.

We gratefully acknowledge the support of S. D. Price, who has maintained GLADYS at the Geophysics Directorate of the Air Force's Phillips Laboratory and has been a significant force behind this research. The staff at WIRO have also been very helpful. S. Kleinmann, S. Sandford, A. Tielens, R. Stencel, and T. Roush have all contributed to this manuscript through their discussions with the authors. F. Witteborn and T. Roellig made useful comments on the manuscript. This investigation made use of the LRS database in Calgary, the SIMBAD database in Strasbourg, and data distributed by NASA's Astronomical Data Center. G. Sloan was supported during this research by the Geophysics Scholar and Phillips Lab. Scholar programs and by the National Research Council.

REFERENCES

Bregman, J. D., Campins, H., Witteborn, F. C., Wooden, D. H., Rank, D. M., Allamandola, L. J., Cohen, M., & Tielens, A. G. G. M. 1987, A&A, 187, 616
Cohen, M., Walker, R. G., & Witteborn, F. C. 1992, AJ, 104, 2030
Cohen, M., Witteborn, F. C., Walker, R. G., Bregman, J. D., & Wooden, D. H. 1995, AJ, 110, 275
Draine, B. T. 1985, ApJS, 57, 587
Draine, B. T., & Lee, H. M. 1984, ApJ, 285, 89
Forrest, W. J., Gillett, F. C., & Stein W. A. 1975, ApJ, 195, 423
Gillett, F. C., Forrest, W. F., Merrill, K. M., Capps, R. W., & Soifer, B. T. 1975, ApJ, 200, 609
Gillett, F. C., Low, F. J., & Stein, W. A. 1968, ApJ, 154, 677
Gilman, R. C. 1969, ApJ, 155, L185
Glaccum, W. 1995, in ASP Conf. Proc. 73, Proc. Airborne Astronomy Symp. on the Galactic Ecosystem: From Gas to Stars to Dust, ed. M. R. Haas, J. A. Davidson, & E. F. Erickson (San Francisco: ASP), 395
Habing, H. J. 1988, A&A, 200, 40
———. 1990, in From Miras to Planetary Nebulae: Which Path for Stellar Evolution?, ed. M. O. Mennessier & A. Omont (Gif-sur-Yvette: Editions Frontières), 16
Hackwell, J. A. 1972, A&A, 21, 239
Hoffmeister, C., Richter, G., & Wenzel, W. 1984, Variable Stars (Berlin: Springer)
Iben, I., Jr., & Renzini, A. 1983, AR&A, 21, 271
IRAS Point Source Catalog, Version 2.0. 1988, Joint *IRAS* Science Working Group (Washington: GPO) (PSC)
IRAS Science Team 1986, A&AS, 65, 607 (LRS Atlas)
Jura, M., & Kleinmann, S. G. 1989, ApJ, 341, 359
———. 1992a, ApJS, 79, 105
———. 1992b, ApJS, 83, 329
Jura, M., Yamamoto, A., & Kleinmann, S. G. 1993, ApJ, 413, 298
Kerschbaum, F., & Hron, J. 1992, A&A, 263, 97
Kholopov, P. N., et al. 1985–1988, General Catalogue of Variable Stars (4th ed.; Moscow: Nauka and Greenbelt: NASA Astronomical Data Center) (GCVS)
Little-Marenin, I. R., & Little, S. J. 1988, ApJ, 333, 305
———. 1990, AJ, 99, 1173
Little-Marenin, I. R., & Price, S. D. 1986, in Summer School on Interstellar Processes: Abstracts of Contributed Papers, ed. D. J. Hollenbach & H. A. Thronson (NASA Technical Memorandum 88342), 137
Merrill, K. M., & Stein, W. A. 1976a, PASP, 88, 285
———. 1976b, PASP, 88, 294
———. 1976c, PASP, 88, 874
Nuth, J. A., & Hecht, J. H. 1990, Ap&SS, 163, 79
Onaka, T., de Jong, T., & Willems, F. 1989, A&A, 218, 169
Ossenkopf, V., Henning, T., & Mathis, J. S. 1992, A&A, 261, 567
Sandford, S. A., & Walker, R. M. 1985, ApJ, 291, 838
Simpson, J. P. 1991, ApJ, 368, 570
Sloan, G. C., Grasdalen, G. L., & LeVan, P. D. 1993, ApJ, 404, 328
Sloan, G. C., & Price, S. D. 1995, ApJ, 451, 758 (Paper I)
Stencel, R. E., Nuth, J. A., Little-Marenin, I. R., & Little, S. J. 1990, ApJ, 350, L45
Tielens, A. G. G. M. 1989, in From Miras to Planetary Nebulae: Which Path for Stellar Evolution?, ed. M. O. Mennessier & A. Omont (Gif-sur-Yvette: Editions Frontières), 186
Toon, O. B., Pollack, J. B., & Khare, B. N. 1976, J. Geophys. Res., 81, 33
Treffers, R., & Cohen, M. 1974, ApJ, 188, 545
Vardya, M., de Jong, T., & Willems, F. 1986, ApJ, 304, L29
Woolf, N. J., & Ney, E. P. 1969, ApJ, 155, L181